Int. J. Electrochem. Sci., 8 **(2013)** 2354 - 2364

International Journal of
ELECTROCHEMICAL
SCIENCE
www.electrochemsci.org

Effect of Bath Temperature on the Microstructural Properties of Electrodeposited Nanocrystalline FeCo Films

Wei Lu[1,*], *Ping Huang*[1], *Kaikai Li*[1], *Pengfei Yan*[1], *Yuxing Wang*[2] *and Biao Yan*[1]

[1] School of Materials Science and Engineering, Shanghai Key Lab. of D&A for Metal-Functional Materials, Tongji University, Shanghai 200092, China
[2] Department of Chemicals and Materials Engineering, The University of Auckland, PB 92019, Auckland, New Zealand
[*]E-mail: weilu@tongji.edu.cn

Received: 24 December 2012 / *Accepted:* 17 January 2013 / *Published:* 1 February 2013

In this paper, FeCo films (55~80 at.% Co) were electrodeposited at different bath temperatures. With increasing bath temperature, the Co content is increased while Fe content is decreased. Elevated bath temperature promotes the formation of metastable α-Mn phase (50~80 ^{o}C) while the fcc solid solution forms at low temperature (less than 30 ^{o}C). The bcc α-Co_7Fe_3 phase is favored at intermediated temperature (RT~50 ^{o}C). However, a mixed phase (bcc + fcc) is formed in FeCo film electrodeposited at 90 ^{o}C. XANES results are consistent well with XRD data. In addition, higher bath temperature leads to a small decrease in the lattice parameters of both bcc phase and α-Mn type $Co_{0.72}Fe_{0.28}$ phase. With increasing bath temperature, the averaged grain sizes of fcc phase and bcc phase decrease while that of α-Mn type $Co_{0.72}Fe_{0.28}$ phase increase. The surfaces of the electrodeposited films are generally quite smooth, uniform and compact, with small particles which become larger as the bath temperature is increased.

Keywords: FeCo film; electrochemical deposition

1. INTRODUCTION

The processing, microstructure and properties of metallic materials with grain size in the tens to several hundreds of nanometer range are of great interest for researchers over the past decades. In recent years, there has been tremendous interest in the development of nanocrystalline materials with grain sizes lower than 100 nm. [1] These materials often benefit from enhanced and sometimes novel, chemical and physical properties comparing with their conventional polycrystalline counterparts. An enhancement in hardness, fatigue behavior, magnetic properties, wear and corrosion resistance is often observed from the reduction in the grain size toward the sub-100 nm scale.

Nanocrystalline FeCo alloys of various compositions are important magnetic materials due to its high saturation magnetization, high permeability, low coercivity, and good thermal stability that cannot be matched by any other alloy system. They have been used widely and commercially in magnetic sensors, magnetic recording head, motors, and generators in electric vehicles.[2-4] Recently, researches for fabrication and properties of FeCo based alloy films have attached more attention. As compared to different deposition methods for the nanocrystalline metallic films, electrodeposition has always been a well accepted method [5-9], due to its relatively higher efficiency, easier control and lower cost. Electrodeposition of FeCo alloy films is one of the most popular fabrication processes for its low cost and simple, flexible operation, inexpensive apparatus and easy reliable control by changing the parameters in the whole electrodeposition process although stable plating baths are needed for commercial processing. Moreover, it is generally compatible with the fabrication of magnetic components with irregular shapes in integrated devices [10].

In electrodeposition, the growth mechanism, morphology and microstructure and physical properties of the films depend on electrodeposition conditions such as electrolyte pH, temperature, deposition potential and electrolyte composition.[11-14] The deposition temperature was observed to change significantly the microstructure, morphology and magnetic properties of electrodeposited films [15, 16]. It is well known that the magnetic properties of Fe-Co films are greatly affected by their compositions and microstructures [2-4], thus a reliable control of the composition and microstructure is an important issue in designing the magnetic functionality of these materials.

Despite continuing research efforts [17-19], the effect of bath temperature on the structural properties and electrodeposition behavior for co-electrodeposited FeCo alloy films has not been fully studied. In present study, the effect of bath temperature on the composition, phase structure and morphology of electrodeposited FeCo films were investigated by using X-ray Diffraction (XRD), scanning electron microscope (SEM) equipped with energy dispersive spectrometer (EDS) and X-ray absorption spectroscopy (XAS).

2. EXPERIMENTAL

FeCo thin films were fabricated by co-electrodeposition from sulfate bath using a conventional three electrode cell. The copper plate serves as the working cathode with the surface area of $1cm^2$ while a graphite plate serves as the anode with much larger surface area. Prior to deposition, the substrate was first mechanically polished, then washed in 10% H_2SO_4 and distilled water. The reference electrode was a saturated calomel electrode.

The compositions of the electrolytes of Co^{2+}/Fe^{2+} were shown in Table 1, together with major electrodepositing parameters. The total concentration of ferrous sulfate [$FeSO_4 \cdot 7H_2O$] and cobalt sulfate [$CoSO_4 \cdot 7H_2O$] was kept 0.35 mol/L. All chemicals were reagent grade and dissolved in distilled water. The electrodeposition was conducted at different bath temperatures (room temperature to 90 ^oC) with a certain stirring rate.

The crystallographic structure of electrodeposited FeCo films was characterized by X-ray Diffraction (XRD). The compositions of the samples were detected through energy dispersive

spectrometer (EDS). Field-emission scanning electronic microscopy (FESEM) was employed to examine the morphology of the films.

Table 1. Compositions of the electrolytes and major electrodepositing parameters

Composition	pH	Current density (mA/cm^2)
$CoSO_4.7H_2O$ (0.2mol/L)		
$FeSO_4.7H_2O$ (0.15mol/L)		
Na_2SO_4 (0.7mol/L)	3	10
Ascorbic Acid (0.05mol/L)		
Boric acid (0.4mol/L)		

X-ray absorption near edge spectroscopy (XANES) measurements on electrodeposited films corresponding to the energy of Fe and Co $L_{3,2}$-edges was performed at beamline 14W of Shanghai Synchrotron Radiation Facility (SSRF).

3. RESULTS AND DISCUSSION

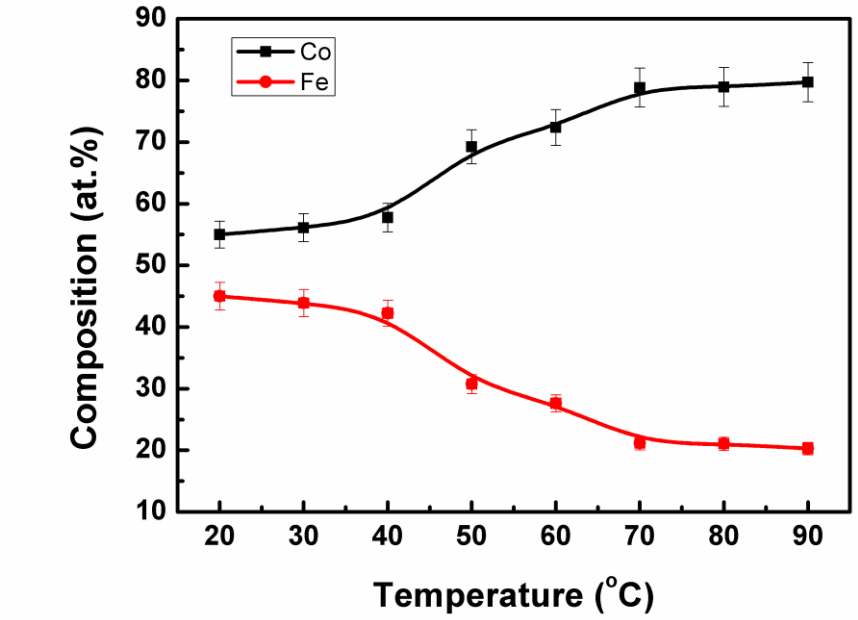

Figure 1. Composition of co-electrodeposited FeCo alloy films at different bath temperatures

The composition of co-electrodeposited FeCo alloy films at different bath temperatures is shown in Fig.1. As can be seen, the Fe concentration in the co-deposited films is decreased from around 45 at.% to 20 at.% when the bath temperature is increased from 20 ^{o}C to 90 ^{o}C. The molar ratio of Co:Fe in the bath solution was 4:3, which should result in electrodeposited films with compositions of ~43 at% Fe (~57 at% Co) assuming non-preferential co-electrodeposition. Thus, it can be suggested that Fe is preferentially deposited when the bath temperature is set as 20 ^{o}C, relative to the composition of electrolyte solution, at the expense of Co. Iron has a lower reduction potential than Cobalt. Therefore, the results indicate slightly anomalous co-electrodepositing behavior for the electrolyte solution at 20 ^{o}C. This so-called anomalous co-deposition has long been reported [20-22]. A hydroxide-based model for the anomalous co-deposition was first proposed by Dahms and Croll [23]. This model was modified later by emphasizing the role of ionized hydrolysis products [24, 25]. Recent researches indicated that the electrode kinetics, such as the adsorption of monovalent ions intermediates on the electrode, plays a more important role than the chemical reactions in the solution and it is thought to be the result of an inhibiting effect of Fe on the nucleation and growth of Co on the cathode surface. [26-28] The bath temperature should show a significant effect on the deposit composition due to a strong dependence of the surface adsorption on temperature [29]. When the bath temperature is increased to 30~40 ^{o}C, the composition of the deposits closely reflects the solution composition, while at temperature higher than 40 ^{o}C, the deposited films become Co-rich. At high temperatures (e.g., 50 ^{o}C), the behavior is as normally expected since the more noble metal (Co) is deposited preferentially; as a result, electrodeposited films contain more Co than the electrolyte composition.

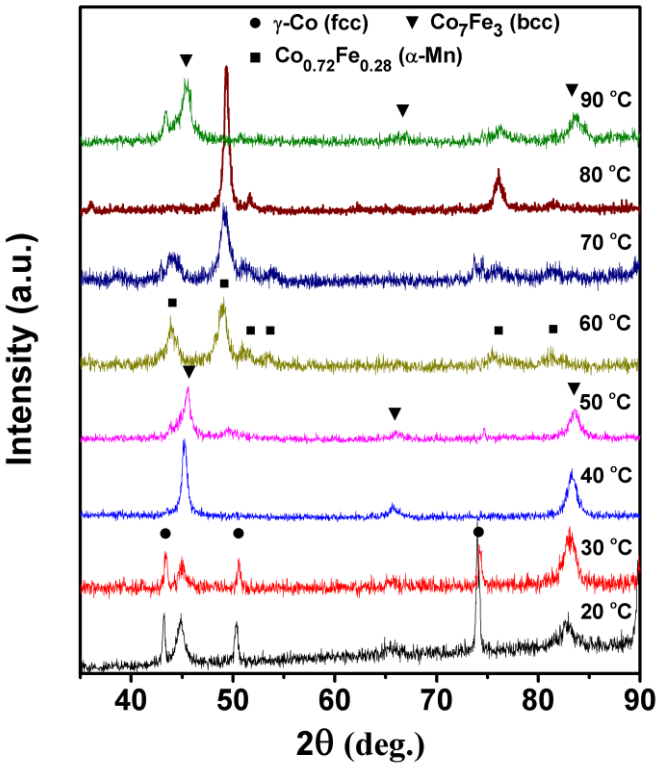

Figure 2. XRD patterns of FeCo films electrodeposited at different bath temperatures

Concerning a successful application of the electrodeposited FeCo alloys, not only the composition but also the microstructure has to be controlled precisely. One of the most important microstructure issues is the phase structure, since both the superior magnetic and mechanical properties depend strongly on it. Fig.2 shows the XRD patterns of FeCo films electrodeposited at different bath temperatures. From the patterns, it can be seen that the films have a mixed phases of face-centered cubic (fcc) solid solution (γ phase), body-centered cubic (bcc) α-Co_7Fe_3 phase (α-Fe type), $Co_{0.72}Fe_{0.28}$ phase with α-Mn structure and hcp Co phase. As seen from the figure, the reflections from the characteristic (111), (200) and (220) crystal planes of fcc CoFe solid solution phase were observed at approximately $2\theta=44^o$, 51^o and 75^o, respectively. In addition, the (110), (200), (211) peaks of bcc α-Co_7Fe_3 phase were observed at about 45^o, 66^o and 84^o, respectively. The patterns indicate that the film electrodeposited at RT~30 ^{o}C has a mixed phase of fcc and bcc phases. As the bath temperature increases, the fcc phase transforms to bcc phase and the characteristic peaks of fcc phase disappear at the bath temperature of 40 ^{o}C. The structure becomes completely bcc for the films deposited at 40 ^{o}C as seen from Fig. 2. As the bath temperature is increased to 50 ^{o}C, the characteristic peaks of metastable α-Mn type $Co_{0.72}Fe_{0.28}$ phase are observed. Further increasing the bath temperature to 60 ^{o}C, the peaks of metastable $Co_{0.72}Fe_{0.28}$ phase are detected strongly at peak positions of 44°,50°,52°,55°,76°and 81° while the peaks of bcc solid solution phase become very weak and nearly can not be detected. When the temperature is increased further to 70~80 ^{o}C, the bcc solid solution phase disappears completely and only the peaks of α-Mn type phase can be indexed. However, when the bath temperature is increased to 90 ^{o}C, the metastable $Co_{0.72}Fe_{0.28}$ phase disappears while bcc and fcc phase are clearly observed. Results indicate that the fcc and bcc FeCo solid solutions form at lower temperatures and low Co concentrations while the metastable α-Mn phase is favored at high temperature and high Co concentrations. A two-phase mixed structure of the α-Mn phase and the bcc solid solution phase forms for intermediate conditions (50 ^{o}C).

According to the phase diagram of Fe-Co binary alloy [30], fcc solid solution phase is thermodynamically stable for high Co concentration (>90 at%) at low temperature (<700 ^{o}C) or for all alloy concentrations at temperatures between ~985 ^{o}C and ~1475 ^{o}C while bcc α phase is stable for Fe concentrations in excess of 80 at% at temperatures below 500 ^{o}C. The binary phase diagram gives a good indication of the phases that might be expected in Fe–Co thin films at a particular composition. However, although thermodynamically stable at low temperature and over a wide composition range (25~75 at% Fe) according to the phase diagram (Fig. 1), the α' phase is never observed in our electrodeposited thin films and other researches [2-4, 31, 32]. It is reported [2-4, 31, 32] that under many electrodepositing conditions the fcc Fe-Co solid solution phase and bcc α phase form during electrodeposition. The formation of non-equilibrium phases of the two solid solution phases is not surprising for electrodeposition systems as the deposition rates do not provide sufficient time for the ordering of Co and Fe atoms on specific lattice positions to form α'-CoFe phase. In our work, for electrodeposition of FeCo films with Co concentrations ranging from around 55 to 80 at% at all bath temperatures, the fcc solid solution was only detected for the bath temperature of low temperatures (less than 30 ^{o}C) and high temperature (higher than 90 ^{o}C) while the bcc phase was obtained for bath temperature from 20 to 50 ^{o}C. The metastable $Co_{0.72}Fe_{0.28}$ phase formed at elevated bath temperatures (50~80 ^{o}C). According to Zhou et al. [21], the formation of the α-Mn type phase is temperature

dependent, and not composition dependent, as the α-Mn type formed at 40 and 60 ^{o}C in their deposited films containing 36–85 at% Co. The electrodeposited films studied in present experiment fall all within this composition range (Fig.1), but no α-Mn type phase formed at low temperatures (RT~40 ^{o}C) and high temperature (90 ^{o}C), consistent with the results of Zhou et al. [21]

It is well established that XANES spectrum gives information on the local atomic structure around the absorbing atom and it may be used qualitatively as a fingerprint of the crystallographic structure by comparing the spectrum of known reference with XANES profiles of the samples. Normalized Fe *K* edge and Co K edge XANES spectra measured for FeCo alloys electrodeposited at different bath temperatures are shown in Fig.3.

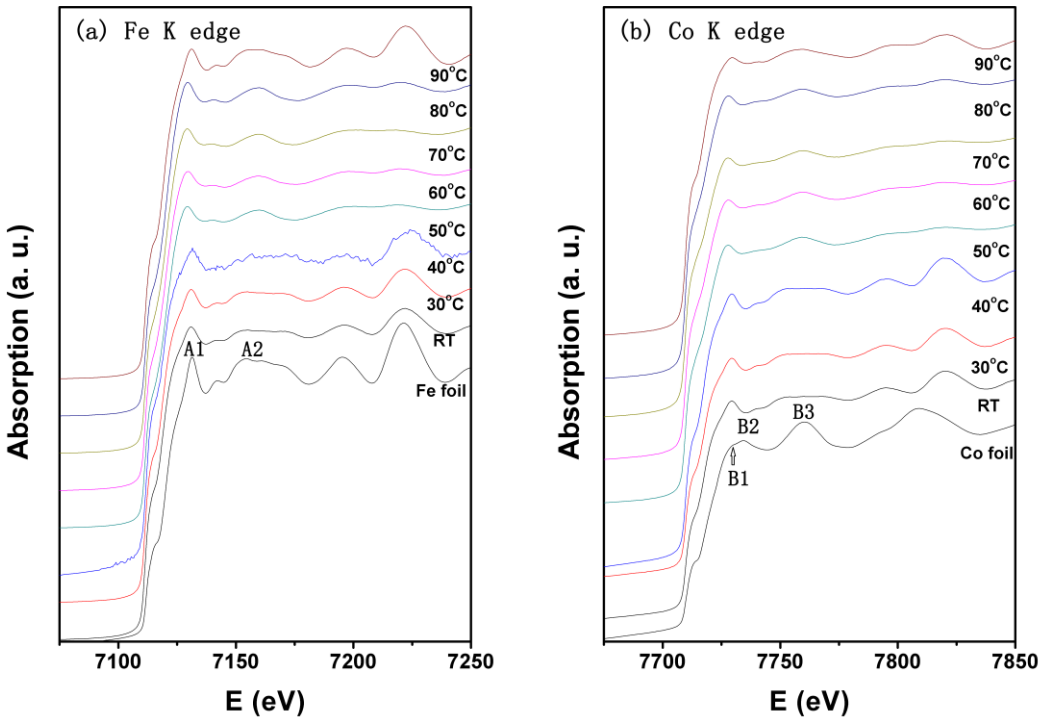

Figure 3. Normalized Fe *K* edge and Co K edge XANES spectra measured for FeCo alloys electrodeposited at different bath temperatures

The spectra of the polycrystalline Fe and Co foil are given for comparison. The bcc symmetry in pure Fe is characterized by a two-peak structure labeled A1 and a smooth structure labeled A2. Three peaks labeled B1, B2, and B3 are characteristic of the hcp and fcc symmetry. The data for all edges in the figures are plotted on the same energy scale. The upper spectra are shifted vertically for clarity.

Comparing the features of the Fe *K* edge spectra of the FeCo samples with the bcc reference Fe we see that all shapes are very similar, while overall amplitudes are smeared out indicating a poor crystalline order. These features do not change significantly until the bath temperature is increased up to 60 ^{o}C. After the bath temperature is increased higher than 60 ^{o}C, namely, the shapes of the peaks are different from that of Fe foil and show an obvious structural change. When the bath temperature is set

as 90 ^{o}C, the features of the Fe *K* edge spectra is similar to that of Fe foil again. Therefore, The structure of the Fe in the FeCo films electrodeposited at low bath temperatures (RT~50 ^{o}C) is thus bcc, starting with a poor crystallinity for sample electrodeposited at lower bath temperature, and evolving with an improvement of the crystallinity after increasing the bath temperature. Further increasing the bath temperature (60~80 ^{o}C), the structure of the Fe in the FeCo films is no longer bcc. However, when the bath temperature is increased to 90 ^{o}C, the Fe *K* edge XAFS data reveal a local coordination geometry consistent with that of a bcc structure again. These results are consistent with what was observed by XRD.

On the other hand, for Co *K* edge (shown in Fig. 3(b)) the spectra(RT~50 ^{o}C) exhibit oscillations very closely that of the Fe reference. The data indicate that the Co in the FeCo films electrodeposited at RT~50 ^{o}C and 90 ^{o}C adopts a bcc structure, as can be seen by visual comparison with Fe reference. While the characteristics of Co *K* edge XAFS data from FeCo films electrodeposited at 60~80 ^{o}C indicate an unknown structure. The bcc ‘‘fingerprint’’ of the Co atoms in the Co *K* edge XANES in the FeCo films is clearly evidenced, although the occurrence of a bcc Co phase is not expected.

Table 2. Average lattice parameters (nm) of bcc phase and α-Mn type $Co_{0.72}Fe_{0.28}$ phase in FeCo films prepared at different bath temperatures

T (^{o}C) / phase	20	30	40	50	60	70	80	90
Co_7Fe_3(110)	0.2854	0.2842	0.2830	0.2809				0.2814
$Co_{0.72}Fe_{0.28}$(332)					0.8725	0.8692	0.8655	

The lattice parameters of the electrodeposited phase in films were calculated based on the peak positions in the XRD patterns. Table.2 shows the average lattice parameters of bcc phase and α-Mn type $Co_{0.72}Fe_{0.28}$ phase in alloy films prepared at different bath temperatures. Higher bath temperature leads to a small decrease in the lattice parameter for the bcc phase. This is to be expected due to the slightly smaller atomic radius of the Co atoms and enrichment of Co content in bcc phase. The incorporation of small atoms into the lattice of the film would shrink the lattice and decrease the lattice parameters. The lattice parameter of the α-Mn type $Co_{0.72}Fe_{0.28}$ phase also slightly decreases when the bath temperature is increased. This may indicate a slight enrichment of Co in the $Co_{0.72}Fe_{0.28}$ phase of film electrodeposited at bath temperature higher than 60 ^{o}C. This results in a reduction in the lattice parameter of α-Mn type $Co_{0.72}Fe_{0.28}$ phase.

Table 3. Averaged grain sizes (nm) of fcc phase, bcc phase and α-Mn type $Co_{0.72}Fe_{0.28}$ phase in FeCo films prepared at different bath temperatures

T (°C) / phase	20	30	40	50	60	70	80	90
γCo(220)	61.8	36.9						
Co_7Fe_3(110)	23.9	21.3	20.3	16.5				10.8
$Co_{0.72}Fe_{0.28}$(332)					18.2	18.6	28.2	

By using Scherer equation, the averaged grain sizes of fcc phase, bcc phase and α-Mn phase in FeCo films electrodeposited at different temperatures are calculated and shown in Table.3. It can be seen that with increasing bath temperature (from 20 °C to 30 °C), the averaged grain sizes of fcc phase decrease from around 62 nm to 37 nm. The decrease in grain size of fcc phase probably caused by the competitive growth of grains in the mixed phase of fcc and bcc phases. With increasing bath temperature (from 20 °C to 50 °C), the grain size of bcc phase decrease from around 24 nm to 16.5 nm. At the bath temperatures in which the size of critical clusters is in atomic dimension, every active site can act as a critical nucleus. So, the thermodynamic barriers for nucleus formation are negligible and the grain size of deposit is controlled by kinetics variables.[33] In such conditions, according to Arrhenius equation, the nucleation rate increases by increasing the bath temperature [34] leading to finer bcc phase grain in our present work. Further increasing the bath temperature, the bcc phase transforms to α-Mn type $Co_{0.72}Fe_{0.28}$ phase and the corresponding averaged grain sizes of α-Mn type $Co_{0.72}Fe_{0.28}$ phase increase from about 18 nm (60 °C) to 28 nm (80 °C). It is known that the energy of grain nucleus formation depends on the cathodic overpotential [33]. A large cathodic overpotential reduces the energy of nucleus formation, and therefore increases the nucleus densities (the number of nucleus per surface area) and refines the grains of the coating. Consequently, since the cathodic overpotential decreases with increasing the bath temperature [35, 36],it is expected that the grain size of the $Co_{0.72}Fe_{0.28}$ phase increases.

Fig. 4 shows the surface morphology of FeCo films electrodeposited at various bath temperatures. The surfaces of the electrodeposited films are generally quite smooth, uniform and compact, with small particles which become larger as the bath temperature is increased. Although the particles are similar to grains in appearance, TEM analysis (not shown in current study) indicates that the actual grain size is much smaller than the partcile sizes. It is interesting to see that a colony-like morphology which consists of a lot of grain colonies is observed for the FeCo film electrodeposited at 60 °C. Each colony could be found to contain several smaller grains. But the small grains cannot be distinguished in Fig.4 (g) because of the poor resolution of the SEM image.

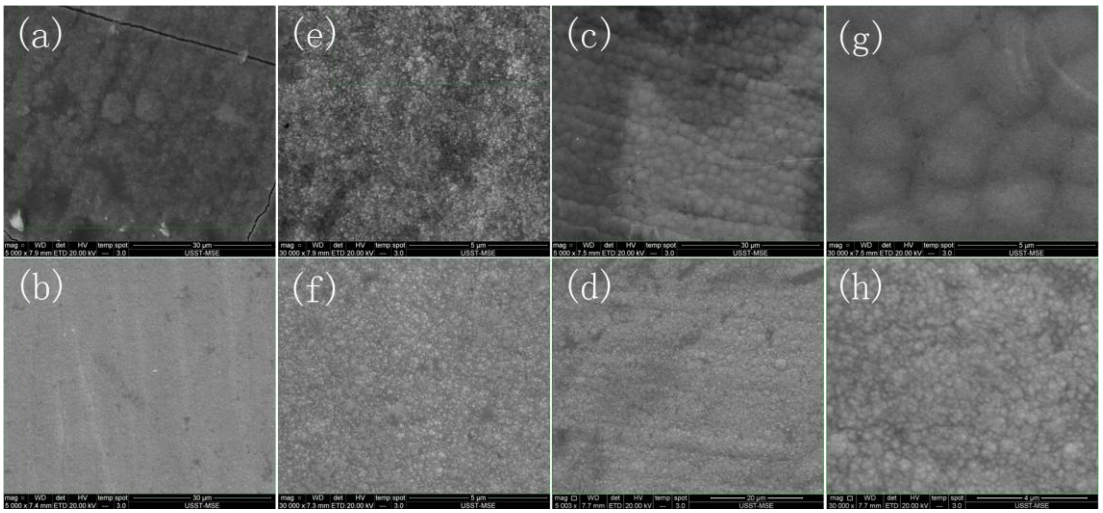

Figure 4. Surface morphology of FeCo films electrodeposited at various bath temperatures. (a)/(e):RT; (b)/(f):40 ^{o}C; (c)/(g):60 ^{o}C; (d)/(h):80 ^{o}C.

In addition, cracks were observed in the electrodeposited FeCo film at lower temperature (20 ^{o}C), likely a result of stress relief. Increasing the bath temperature is known to reduce stress in electrodeposited films and has often been attributed to a reduction in the overpotential for electrodeposition of metallic films. A lowering of the overpotential permits the metallic cations to migrate to the cathode surface more easily and allows the opportunity for ad-atoms to migrate to stable kink sites. In addition, a lower overpotential discourages the reduction of hydrogen at the cathode, which has also been shown to increase the residual stresses in electroplated films.

4. CONCLUSIONS

FeCo films (55~80 at.% Co) were electrodeposited at different bath temperatures. The composition of FeCo films is greatly affected by the bath temperatures. With increasing temperature, the Co content is increased while Fe content is decreased. Elevated bath temperature promotes the formation of metastable α-Mn phase (50~80 ^{o}C) while the fcc solid solution forms at low temperature (less than 30 ^{o}C). The bcc α-Co_7Fe_3 phase is favored at intermediated temperature (RT~50 ^{o}C). However, a mixed phase (bcc + fcc) is formed in FeCo film electrodeposited at 90 ^{o}C. XANES results consist well with XRD data. Higher bath temperature leads to a small decrease in the lattice parameters of both bcc phase and α-Mn type $Co_{0.72}Fe_{0.28}$ phase. With increasing bath temperature, the averaged grain sizes of fcc phase and bcc phase decrease while that of α-Mn type $Co_{0.72}Fe_{0.28}$ phase increase. The surfaces of the electrodeposited films are generally quite smooth, uniform and compact, with small particles which become larger as the bath temperature is increased. And cracks were observed only in the electrodeposited FeCo film at lower bath temperature (20 ^{o}C).

ACKNOWLEDGEMENTS
The present work was supported by National Natural Science Foundation of China (Grant No. 50901052, 51071109) and Program for Young Excellent Talents in Tongji University (Grant No. 2009KJ003) and "Chen Guang" project (Grant No.10CG21) supported by Shanghai Municipal Education Commission and Shanghai Education Development Foundation.

References

1. K.S. Kumar, H. Van Swygenhoven, S. Suresh. *Acta Materialia* 51 (2003) 5743
2. K. Sundaram, V. Dhanasekaran, T. Mahalingam, *Ionics* 17 (2011) 835
3. S. Mehrizi , M. Heydarzadeh Sohi, S.A. Seyyed Ebrahimi, *Surface & Coatings Technology* 205 (2011) 4757
4. D. Zhou,M. Zhou, M. Zhu, X. Yang, M. Yue, *J. Appl. Phys*. 111 (2012) 07A319
5. G. Saravanan, S. Mohan, *Int. J. Electrochem. Sci*. 6 (2011) 1468
6. R.Balachandran, H.K.Yow, B.H.Ong, K.B.Tan, K.Anuar, H.Y.Wong, *Int. J. Electrochem. Sci.* 6 (2011) 3564
7. J. A. R. Márquez, C. M. B. Rodríguez, C. M. Herrera, E. R. Rosas, O. Z. Angel, O. T. Pozos, *Int. J. Electrochem. Sci.* 6 (2011) 4059
8. H. B. Hassan, Z. Abdel Hamid, *Int. J. Electrochem. Sci.* 6 (2011) 5741
9. B. Bozzini, D. Lacitignola, I. Sgura, *Int. J. Electrochem. Sci.* 6 (2011) 4553
10. N. V. Myung, D.-Y Park, B.-Y Yoo, Paulo T.A Sumodjo, Journal of Magnetism and Magnetic Materials 265 (2003) 189
11. J.-W. Park, J.-Y. Eom, H.-S. Kwon, *Int. J. Electrochem. Sci.* 6 (2011) 3093
12. G. Orhan , G. Hapci, O. Keles, *Int. J. Electrochem. Sci.* 6 (2011) 3966
13. J.C. Ballesteros, E. Chainet, P. Ozil, Y. Meas, G. Trejo, *Int. J. Electrochem. Sci.* 6 (2011) 2632
14. H. Adelkhani, M. Ghaemi, M. Ruzbehani, *Int. J. Electrochem. Sci.* 6 (2011) 123
15. H. Natter and R. Hempelmann, J. Phys. Chem. 100 (1996) 19525
16. S.M.S.I. Dulal, H. J. Yun, C. B. Shin, C. K. Kim, Electrochimica Acta 53 (2007) 934
17. W. Lu, P. Huang, C. He and B. Yan, *Int. J. Electrochem. Sci.* 8 (2013) 914
18. I. Tabakovic, S. Riemer**,** N. Jayaraju, V. Venkatasamy, J. Gong, *Electrochimica Acta* 58 (2011) 25
19. X. Yang, L. Gong, J.Wei, L. Qiao, T. Wang, F. Li, *J. Phys. D: Appl. Phys.* 43 (2010) 215002
20. X. Liu, P. Evans, G. Zangari, *IEEE Trans. Mag.* 36 (2000) 3479
21. S. Zhou, Q. Liu, D.G. Ivey, *IEEE Int. Nanoelectron. Conf*. 474 (2008) 4585531
22. R. Bertazzoli, D. Pletcher, *Electrochemica Acta*. 38 (1993) 671
23. H. Dahms, I.M. Croll, *J. Electrochem. Soc*. 112 (1965) 771
24. S. Hessami, C.W. Tobias, *J. Electrochem. Soc*. 136 (1989) 3611
25. T.M. Harris, J. St. Clair, *J. Electrochem. Soc.* 143 (1996) 3918
26. M. Matlosz, *J. Electrochem. Soc*. 140 (1993) 2272
27. B.C. Baker, A.C. West, *J. Electrochem. Soc.* 144 (1997) 169
28. N. Zech, E.J. Podlaha, D. Landolt, *J. Electrochem. Soc*. 146 (1999) 2892
29. A.W. Adamson, A.P. Gast, in: Physical Chemistry of Surfaces, 6th ed., John Wiley & Sons, New York, USA (1997)
30. H. Bakar, ASM Handbook, Volume 3 Alloy Phase Diagrams, ASM international, Materials Park, Ohio (1992)
31. S. H. Teh, I. I.Yaacob, IEEE TRANSACTIONS ON MAGNETICS 47 (2011) 4398
32. H. Kockar, M. Alper, T. Sahin, O. Karaaga, *Journal of Magnetism and Magnetic Materials* 322 (2010) 1095
33. Y. Li, H. Jiang, W. Huang, H. Tian, *Appl. Surf. Sci*. 254 (2008) 6865
34. J. Vazquez-Arenas, R. Cruz and L.H. Mendoza Huizar: *Electrochim. Acta* 52 (2006) 892

35. H. Natter, R. Hempelmann, *Z. Phys. Chem*. 222 (2008) 319
36. J.W. Dini, Electrodeposition: The Material Science of Coatings and Substrates, Noyes Publications (1993)